

See discussions, stats, and author profiles for this publication at: <https://www.researchgate.net/publication/50941323>

# Shape Dependence of Gold Nanoparticles on In Vivo Acute Toxicological Effects and Biodistribution

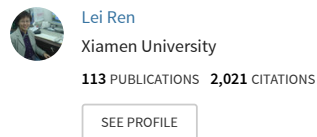
Article in *Journal of Nanoscience and Nanotechnology* · February 2011

DOI: 10.1166/jnn.2011.3094 · Source: PubMed

CITATIONS  
32

READS  
175

5 authors, including:



Some of the authors of this publication are also working on these related projects:



# Shape Dependence of Gold Nanoparticles on *In Vivo* Acute Toxicological Effects and Biodistribution

Ya-Nan Sun<sup>1</sup>, Cai-Ding Wang<sup>1</sup>, Xiu-Ming Zhang<sup>1</sup>, Lei Ren<sup>1,2,\*</sup>, and Xin-Hua Tian<sup>3,\*</sup>

<sup>1</sup>Research Center of Biomedical Engineering, Department of Biomaterials, College of Materials, Xiamen University, Xiamen 361005, P. R. China

<sup>2</sup>State Key Laboratory for Physical Chemistry of Solid Surfaces, Xiamen University, Xiamen 361005, P. R. China

<sup>3</sup>Division of Neurosurgery, Zhong-shan Hospital, Xiamen University, Xiamen 361004, P. R. China

The toxicity and biodistribution *in vivo* of various morphologies of Au nanoparticles (AuNPs) were studied by using KM mice. The quantitative analysis of Au in each tissue of mice was done by using the Inductively Coupled Plasma Mass Spectrometry (ICP-MS). Sphere-shaped AuNPs displayed the best biocompatibility, compared with rod- and cube-shaped of AuNPs, and rod-shaped AuNPs was more toxic than cube-shaped AuNPs. *In vivo* biodistribution study revealed all AuNPs were preferentially accumulated in organ of liver and spleen. The findings from this study thus revealed that the toxicity and biodistribution *in vivo* of AuNPs are shape dependent.

**Keywords:** Au Nanoparticles, *In Vivo*, Toxicity, Biodistribution.

## 1. INTRODUCTION

Gold nanoparticles (AuNPs), which have been known for 2500 years, are the subject of an exponentially increasing number of reports and are full of promises for optical, electronic, magnetic, catalytic, and biomedical applications in the 21st century. In the past decade or so, numerous advances in the chemical synthesis of AuNPs with different size, composition, shape (other than spheres), and structure (solid versus hollow), have opened up even more possibilities for sensing and imaging applications. Furthermore, from the fascination produced by the more or less virtual medical uses of soluble gold in the past millennia, it remains at least that AuNPs are completely biocompatible. AuNPs display several features that make them well suited for biomedical applications, including straightforward synthesis,<sup>1</sup> stability,<sup>2</sup> and the facile ability to incorporate secondary tags such as peptides targeted to specific cell types to afford selectivity.<sup>3</sup> The recent burst of research involving AuNPs as transfection vectors,<sup>4</sup> DNA-binding agents,<sup>5</sup> protein inhibitors,<sup>6</sup> and spectroscopic markers<sup>7</sup> demonstrates the versatility of these systems in biological applications. These nascent technologies rely in part on the excellent elastic light-scattering properties of AuNPs and also on the shift of the plasmon band maxima with local dielectric constant.

The *in vitro* success of cancer therapy/imaging using visible light absorbing nanoparticles can be extended to

Delivered by  skin or surface type cancers. However, *in vivo* imaging and photothermal therapy applications for deeper tissue require light in the near-infrared (NIR) region where tissue (hemoglobin and water) has the highest transmissivity. The light penetration depth can be up to a few centimeters in the spectral region 650–900 nm, also known as the biological NIR window, depending on the tissue type. Thus the surface plasmon resonance (SPR) of AuNPs for *in vivo* applications is required to be in the NIR region. For instance, a colloidal solution of Au nanospheres with a diameter of 50 nm possesses an intense ultraviolet-visible (UV-vis) light extinction band centered on 520 nm, whereas changing the shape and composition of AuNPs offers dramatic variation in SPR absorption and scattering properties. Interesting nanostructures, such as silica-Au nanoshells, Au nanorods, Au nanocages, and Au nanoparticle assemblies show optical tunability in the NIR region suitable for *in vivo* applications. For instance, Huang et al. employed Au nanorods conjugated to anti-EGFR antibodies for NIR cancer cell imaging and selective photothermal therapy,<sup>8</sup> and Xia et al. used Au nanocages in optical coherence tomography and photothermal treatment.<sup>9</sup>

It is evident that, for any clinical application, biocompatibility of the nanoparticles is crucial. Recent observations in cell culture systems suggest that the cellular uptake of gold NPs was heavily dependent upon size and shape, and spherical-shaped particles have a higher probability of entering the cell in comparison to rod-shaped nanostructures.<sup>10–14</sup> Despite the scientific

\*Authors to whom correspondence should be addressed.

literature available on cytotoxicity and immunotoxicology of AuNPs, to our knowledge, little attention has been focused on the *in vivo* experiment to AuNPs. A systematic and thorough quantitative analysis of the pharmacokinetics (absorption, distribution, metabolism, and excretion; PK) of nanostructures can lead to improvements in design of nanostructures for diagnostic and therapeutic applications. PK gives the quantitative *in vivo* conditions under which the dose achieves or causes any observed toxic effects. Toxicity to specific cell types can be qualified by PK in that the time and concentrations to which they will be exposed can be determined. It has been reported that the distribution of gold nanoparticles is size-dependent, the smallest particles showing the most widespread organ distribution including blood, heart, lungs, liver, spleen, kidney, thymus, brain, and reproductive organs,<sup>15–20</sup> but research for different shapes exposure of AuNPs have little report. In this paper, the mice were exposed to AuNPs with different shape via intravenous administration, the nanotoxicity *in vivo* as well as differences in biodistribution of those AuNPs are investigated comparatively on mass basis. The findings from this study will lead to improvements in the design of optimal AuNP for various biomedical applications.

## 2. EXPERIMENTAL DETAILS

### 2.1. Synthesis

AuNPs were generated by an established reduction method as reported previously.<sup>21</sup> In brief, sphere-shaped AuNPs with sizes 50 nm were prepared by the citrate reduction of chloroauric acid. In this method, 300  $\mu$ l of 1% chloroauric acid (HAuCl<sub>4</sub>) was added to 30 ml of doubled distilled water and brought to boil. Next, 1 ml of 1% sodium citrate aqueous solution was added quickly to the HAuCl<sub>4</sub> solution to produce nanoparticles. Refluxing of the solution continued until the color of the boiling solution changes from dark purple to red vine color.

Rod and cube-shaped gold nanoparticles were synthesized with hexadecyltrimethylammonium bromide (CTAB) surfactant. In this reaction, Au seeds were firstly prepared by respectively mixing 0.25 ml HAuCl<sub>4</sub> (0.01 M), NaBH<sub>4</sub> (0.01 M) and 7.5 ml CTAB (0.01 M). In rod-shape AuNPs growth reaction, 1 ml of HAuCl<sub>4</sub> (0.01 M) was added to 23.75 ml of CTAB (0.01 M) at 25 °C. To this solution, 0.3 ml of AgNO<sub>3</sub> (0.01 M), 0.16 ml of L-ascorbic acid (0.01 M) and 0.025 ml of Au seed ( $1.5 \times 10^{-7}$  M) were added in order under gently stirring. The synthesis method for cube-shaped was similar to that for rod-shaped AuNPs, except that AgNO<sub>3</sub> was not used in the system, and the corresponding reaction conditions were CTAB (0.016 M), Au seed ( $2 \times 10^{-8}$  M), HAuCl<sub>4</sub> (0.0002 M), L-ascorbic acid (0.006 M).

The morphological examination of the as-synthesized AuNPs was performed by SEM (LEO1530). Absorption

spectra of the prepared solutions were measured using a UV-vis spectrophotometer (Beckman, DU 800).

### 2.2. Hemolysis Assay

AuNPs were tested for limited hemocompatibility *in vitro*. A hemolysis test was done by modification of direct contact method.<sup>22</sup> In short, blood from healthy New Zealand rabbits was collected in 0.5 ml heparin sodium (300 U). 8 ml of heparinized blood was then diluted by 10 ml saline solution. Saline solution and deionized water were taken as negative (0% hemolysis) and positive (100% hemolysis) control, respectively. All the test specimens were placed in water bath at 37 °C for 30 min. After that, 0.2 ml of heparinized and diluted blood were added in each tube and mixed softly, and then placed in the water bath again at 37 °C for 60 min. After incubation, all tubes were centrifuged at 2500 r.p.m. for 5 min and the supernatant was taken for the estimation of the release of hemoglobin. The absorption at 545 nm was measured by spectrophotometer (Beckman, DU800). Each sample was repeated triplicate. The results were calculated according to the equation following:

$$\text{Hemolysis Ratio (HR\%)} = [(QD_{\text{NPs}} - QD_{\text{NC}})/(QD_{\text{PC}} - QD_{\text{NC}})] \times 100\%$$

### 2.3. Toxicity *In Vivo*

KM mice (provided by Anti-Cancer Research Center, Xiamen University), aged 7 weeks and weighting 18–22 g, were used in *in vivo* experiments. All animal experiments were performed in compliance with the local ethics committee. Following the method provided by the Organization for Economic Cooperation and Development (OECD, guideline 425),<sup>23</sup> a series of doses were set (Table I) to process the toxicological studies *in vivo* of AuNPs. The first mouse received a dose one step below the assumed estimate of the LD<sub>50</sub>. If the animal survived, the second animal received a higher dose. If the first animal dies, the second animal received a lower dose. The signs of toxicity or anaphylactic response after injection of AuNPs were recorded following U.S. Pharmacopeia.<sup>24</sup>

To examine the changes of biochemical parameters, healthy KM mice were exposed by the intravenous injection with the same dose ( $10^7$  grain/g) of various AuNPs, respectively. Blood samples were collected via the ocular vein after exposure up to 14 days, and were then centrifuged twice at 3000 r.p.m. for 10 min in order to separate serum. Alanine aminotransferase (ALT), aspartate aminotransferase (AST), total bilirubin (TB), alkaline phosphatase (ALP), cholinesterase (CHE), albumin (ALB), total protein (TP), creatinine (Cr), and blood urea nitrogen (BUN) levels of serum were measured by a biochemistry analyzer (Hitachi 7080). Each sample was repeated

**Table I.** Acute systemic toxicity *in vivo* for sphere-, cube-, and rod-shaped AuNPs.

	Status	Passive behaviour	Hypopnea	Tremor	Arching of back	Loss of appetite	Diarrhea and vomiting
<b>Sphere</b>							
10 <sup>6</sup> grain/g	Good	No signs	None	None	None	None	None
10 <sup>7</sup> grain/g	Good	No signs	None	None	None	None	None
10 <sup>8</sup> grain/g	Good	No signs	None	None	None	none	none
5 × 10 <sup>8</sup> grain/g	Common	Faintness	None	None	None	None	None
10 <sup>9</sup> grain/g	Common	Median	Faintness	Faintness	None	None	None
<b>Cube</b>							
10 <sup>6</sup> grain/g	Good	None	None	None	None	None	None
10 <sup>7</sup> grain/g	Good	None	None	None	None	None	None
10 <sup>8</sup> grain/g	Common	Faintness	Faintness	None	None	None	None
5 × 10 <sup>8</sup> grain/g	Common	Median	Faintness	Faintness	None	Faintness	None
10 <sup>9</sup> grain/g	Bad	Median	Median	Median	Median	Median	None
<b>Rod</b>							
10 <sup>6</sup> grain/g	Good	None	None	None	None	None	None
10 <sup>7</sup> grain/g	Good	None	None	None	None	None	None
10 <sup>8</sup> grain/g	Good	Faintness	Faintness	None	None	None	None
5 × 10 <sup>8</sup> grain/g	Common	Median	Median	Median	Median	Median	None
10 <sup>9</sup> grain/g	Died	—	—	—	—	—	—

3 times. The differences between the results were analyzed statistically using the two-sample *t*-test.

To examine the pathological changes due to AuNPs injected, the organs of mice such as liver, spleen, lung, and kidney were immediately fixed in 10% formalin and subject to further pathological examinations by dehydrating in a sequence of 50, 70, 95, and 100% ethanol. After clearing in xylene, the tissue was finally embedded in paraffin wax, then 2–3  $\mu$ m sections were sliced using a microtome (Leica RM2235). After histological H-E staining, the slides were observed and the photos were taken using a fluorescent microscope (Olympus BX41).

#### 2.4. Biodistribution *In Vivo*

After filtration through 0.22  $\mu$ m filter membrane, 200  $\mu$ l of AuNPs solution (10<sup>7</sup> grain/g) was injected into a healthy KM mouse via the tail vein, respectively. Samples were taken at 1 or 7 days post-injection from liver, spleen, lung, kidney of KM mice, respectively. Each sample was washed thoroughly with deionized water and dried for 4 h at 120 °C. In order to prepare ICP-MS solution, the samples were digested by a microwave accelerated reaction system (CEM MARS 240/50), following the preset protocols. The digested solutions were then qualitatively analyzed for Au atoms by using an inductively coupled plasma mass spectrometry (ICP-MS, Perkin Elmer, SCIEX ELAN DRC-e). 10 ppb Au aqueous solution (purchased from National Research Center for CRM'S) was used as the standard control. Each sample was repeated five times.

To understand the status of AuNPs injected *in vivo*, the organs of the mice were collected and subsequently fixed with glutaraldehyde at 4 °C for 24 h. After removing the fixatives by 0.1 M PBS, samples were subsequently post-fixed and stained with 1% osmium tetroxide in buffer and then dehydrated in an alcohol series, embedded in Epon,

and sliced to a thickness of 50–70 nm by using a ultra-microtome (LKB Nova). Images of the slices were finally taken with a transmission electron microscope (TEM, JEM 2100) at 120 kV.

### 3. RESULTS AND DISCUSSION

#### 3.1. Preparation and Characterization of AuNPs

Figure 1 show scanning electron microscope (SEM) images of typical samples of various AuNPs and indicate the large quantity and good uniformity that were achieved using these approaches. The spherical AuNPs with ~40 nm in diameter, Au nanocubes had a mean edge length of 50 nm, and the rod-shaped NPs were about 30 nm in width with 80 nm in length. Furthermore, as the morphologies of AuNPs change from sphere-like to rod- or cube-like, their SPR peak was shifted toward longer wavelengths (Fig. 2). It is indicated both of rod- and cube-shaped AuNPs show two absorption bands that are located in the visible region (~520 nm), and in the near-IR region (~700 nm). This unique optical property of Au nanorods and Au nanocubes may open up fascinating their biomedical applications.

#### 3.2. *In Vitro* Hemolysis

Red blood cells (RBCs) are the first cells that come into contact with intravenous administration. *In vitro* erythrocyte-induced hemolysis is considered to be a simple and reliable measure for estimating blood compatibility of materials.<sup>25</sup> The interactions of various nanoparticles with the negatively charged RBCs have been studied by hemolysis experiments,<sup>26</sup> and the behavior of nanoparticles *in vivo* can be predicted by investigating the degree of hemolysis *in vitro*. In this paper, the hemolysis ratio

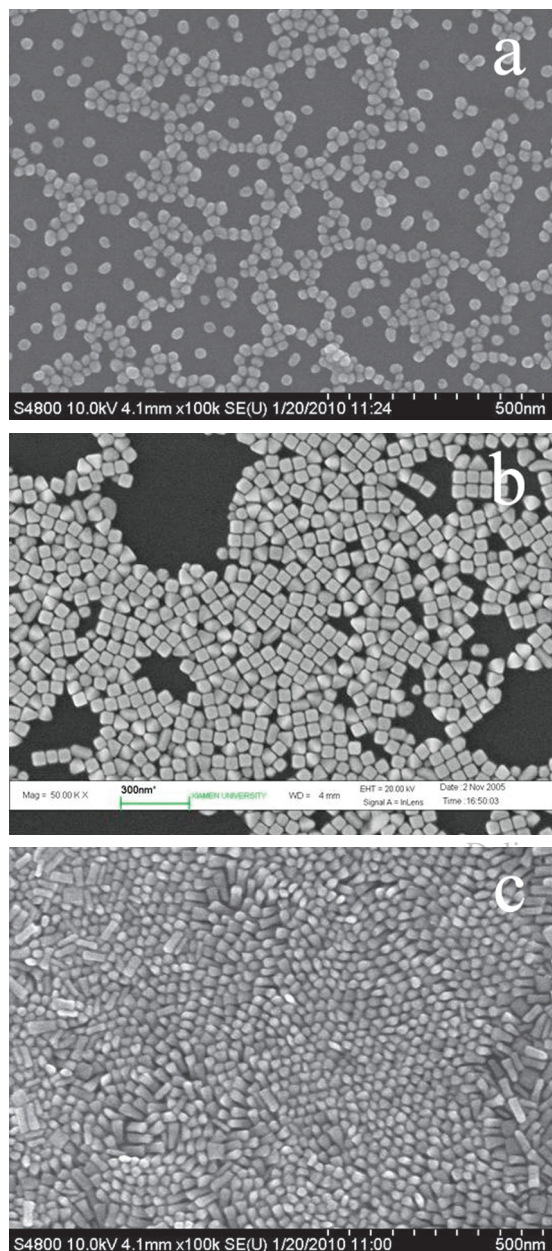


**Fig. 1.** TEM images of (a) sphere-, (b) cube-, and (c) rod-shaped AuNPs.

represents the extent of blood cells broken by AuNPs in contact with blood. The release of hemoglobin was used to quantify the membrane-damaging properties of the AuNPs. As 100% and 0% values we used deionized water and normal saline treated erythrocytes, respectively. It is acceptable that hemolysis ratio (HR%) of biomaterials, which was required for medical applications, must be below 5%.<sup>26</sup> The dose effects of AuNPs on hemolysis were shown in Figure 3. Increasing the mass of AuNPs resulted in enhanced hemolysis ratio. It can be observed that the hemolysis ratio of sphere-shaped AuNPs gently went up to 1.79% with the increase of concentration from  $10^8$  grain/ml to  $10^{10}$  grain/ml. However, upon raising the

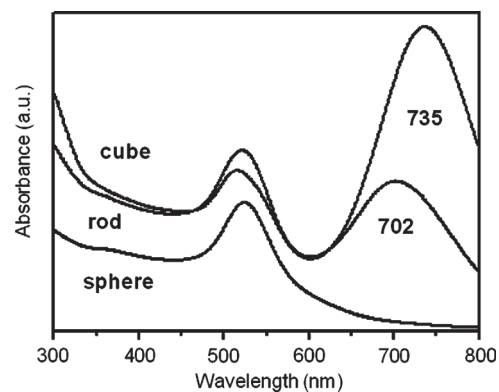


**Fig. 2.** Ultraviolet-visible spectra of AuNPs with (a) sphere, (b) cube, and (c) rod shape.

cube- and rod-AuNPs concentration in the same manner, the hemolysis ratios of AuNPs were increased remarkably, especially when the AuNPs concentration reached up to  $10^{10}$  grain/ml, a distinct hemolysis was visible as presented by cube- and rod-AuNPs, for example, cube-AuNPs got a HR% of 46.67% when rod-AuNPs reach a higher degree of 88.99%. Additionally, at the concentration of  $10^9$  grain/ml, the hemolysis ratios of all shapes of AuNPs were under 5%. As can be seen from the results, there was statistically significant difference between the sphere- and rod-shaped AuNPs, as well as sphere- and cube-shaped AuNPs, respectively. To explain, one must be aware the difference in the surface chemistries (from the stabilizing ligand from the synthesis) between the spherical and rod/cube-shaped gold nanoparticles, and it has been found that the cytoplasm conductivity and the permeability barrier of the cells is affected by the CTAB.<sup>10</sup> We hypothesized that rod- and cube-shaped AuNPs, covered by CTAB, are easier than sphere-shaped AuNPs to affect the membrane of RBC until it breakdown, leading to the subsequent release of hemoglobin like some surface-active chemicals.<sup>12</sup> Nevertheless, it could be concluded that all of these AuNPs with concentration below  $10^9$  grain/ml cause

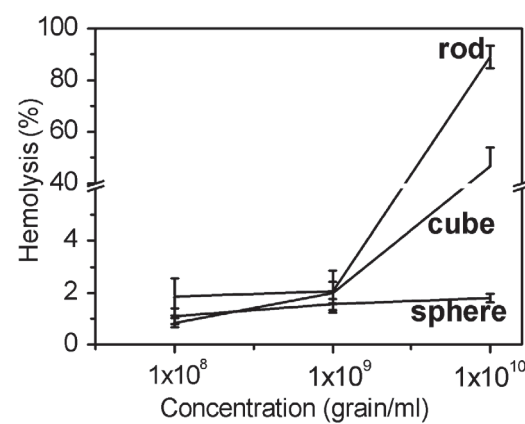


**Fig. 3.** Hemolysis effects as a function of the concentration of (a) sphere-, (b) rod-, and (c) cube-shaped AuNPs. Bars represent the corresponding standard deviations ( $n = 3$ ).

negligible hemolysis (<5%), and could be used for *in vivo* study.

### 3.3. Toxicity *In Vivo*

Acute systemic toxicity studies in animals are usually necessary for any pharmaceutical intended for human use. After several years of debate, the LD50 test was finally deleted by the end of 2002.<sup>27</sup> The Up and Down Procedure<sup>23</sup> has been developed which give rise to significant improvements in animal welfare, which now can be used within a strategy for acute toxicity testing for all types of test substances. Based on this opinion, the experiments we carried out were designed in accordance with the method provided by the OECD guideline 425. The signs of toxicity or anaphylactic response were presented in Table I. It is seen that as the injected sphere-shaped AuNPs concentration varied from  $10^6$  grain/g to  $10^8$  grain/g which dissolved in 0.4 ml PBS, no mice showed any passive behavior, hypopnea, tremor, and arching of back or any symptoms of poisoning such as loss of appetite, diarrhea, and vomiting to these dosages up to 14 days' observation; Whereas the mice showed a tendency of toxicity that exposed to the concentration ranged from  $5 \times 10^8$ – $10^9$  grain/g. Similarly, in the cube- and rod-shaped AuNPs group, no any adverse effect on the treated mice was observed while the dosage was below  $10^7$  grain/g. With increasing the dosage of AuNPs to  $10^8$  grain/g the treated mice in these two groups exhibited a little tendency of toxicity. However, at AuNPs concentration of  $5 \times 10^8$  grain/g and above, the mice in these two groups showed significantly different from each other. In the case of cube-shaped AuNPs group, the mice were median severity when the AuNPs content reached up to  $10^9$  grain/g, but such median severity was observed by the mice in rod-shaped AuNPs group even at a much lower level of  $5 \times 10^8$  grain/g. Upon raising the concentration of rod-shaped AuNPs to  $10^9$  grain/g, all the mice in this group were killed. The above results clearly indicated that at a given concentration, the toxicity of AuNPs *in vivo*

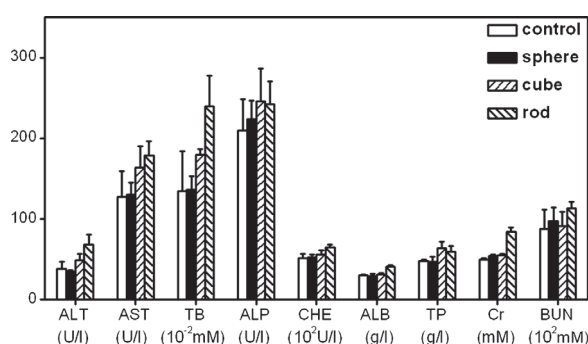


**Fig. 4.** Statistic results of blood biochemical parameters of KM mice exposed to 10 mg/kg of sphere-, cube-, and rod-shaped AuNPs for 7 days, respectively. Control: mice without any treatment.

was strongly dependent on the shape of nanoparticles. This finding is in line with the finding of *In vitro* Hemolysis of AuNPs.

Blood biochemical testing is used extensively both in diseases that have an obvious metabolic basis and those in which biochemical changes are consequence of the diseases.<sup>28</sup> To date most biochemical studies in mice have been used for toxicological testing.<sup>28</sup> The ALT is often tested along with AST, ALP, and LDH to evaluate whether the liver is damaged or diseased. When the liver is in dysfunction, the levels of the above enzymes will rise. The blood BUN and CR are good indicators for renal function. If kidney function falls, the BUN and CR levels will rise. In our experiments, blood biochemical parameters which reflect the hepatic (ALT, AST, TB, ALP, CHE, ALB, TP) and renal (Cr and BUN) functions were further investigated. No statistically significant difference between the control and sphere-/cube-/rod-shaped AuNPs treated mice were observed at 7th day, respectively (Fig. 4). The results suggested that all of the AuNPs did not cause any abnormality in the blood biochemical parameters.

Figure 5 showed the microscopic pictures of liver, spleen, lung, and kidney at 14th day of the injection. There was no inflammation or active immunocyte congregating in these organs. In the case of the liver, the polygonal cells are hepatocytes joined to one another, and the lobule is the structural unit with a central vein (A) in the middle. In terms of spleen, white pulp (B) is equivalent to the lymphocyte population, in the form of the periarteriolar lymphocyte sheath. Red pulp (C) is everything else, which means the splenic cords and the sinuses between them. There are bronchioles, alveolar ducts and alveoli in the lung section, with alveolar cells and capillaries in the alveolar walls. On the kidney section, the renal cortex contains glomeruli (D), other vessels, tubules and interstitium. Thus, no pathological changes were found in each organ such as liver, spleen, lung, and kidney, which showed similar to the control group.

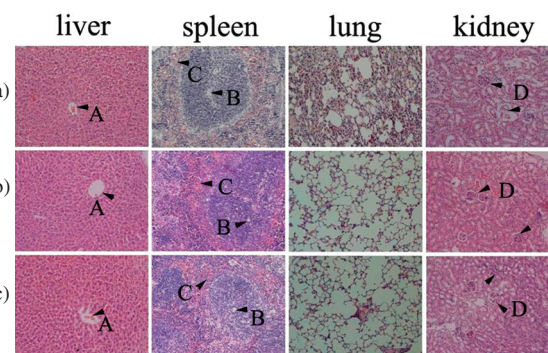


**Fig. 5.** Histopathology assays of liver, spleen, lung, and kidney after injection of (a) sphere-, (b) cube-, and (c) rod-shaped AuNPs at 7 days. Hematoxylin and eosin staining at scope magnifications of 100 $\times$ .

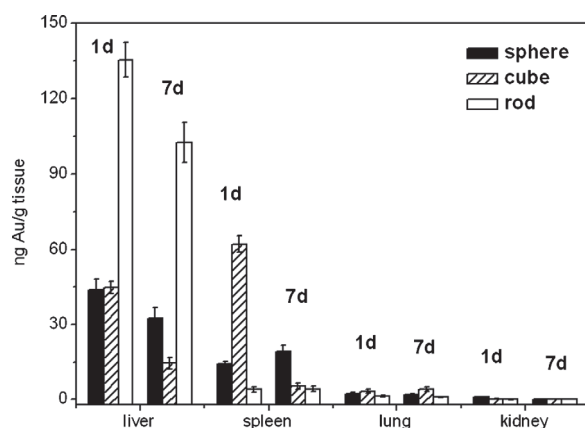


**Fig. 6.** *In vivo* biodistribution of (a) sphere-, (b) cube-, and (c) rod-shaped AuNPs in healthy KM mice after injection for 1 day (1d) and 7 days (7d), respectively.

### 3.4. *In Vivo* Biodistribution of AuNPs

The concentration of Au in each tissue was determined by ICP-MS, and the results of the biodistribution *in vivo* for different AuNPs in healthy mice are presented in Figure 6. Within the whole time post injection, no AuNPs was found in blood, bone, muscle, heart, intestines and brain. AuNPs exhibited the highest uptake in liver and spleen followed by lung and kidney. This was consistent with Yoshifumi's observation that nanoscale substances may be easily taken up by the reticuloendothelial system (RES).<sup>29</sup> On the other hand, it has been shown that nanoparticulate RES uptake can be influenced by altering the surface properties of the particle.<sup>30</sup> As we can see, at the 1st day of injection of AuNPs, most of the rod-shaped AuNPs were found in the liver, while the cube-shaped AuNPs were chiefly located in the spleen. The major sphere-shaped AuNPs distributed in the part of liver and spleen, mainly in liver. However, in lung and kidney, the sphere-shaped AuNPs and the cube-shaped AuNPs distributed a little whereas the rod-shaped were tiny. After injection for 7 days, most of rod-shaped AuNPs deposited in the liver, but some change had happened, cube-shaped AuNPs were much richer in liver than in spleen. In lung and kidney, both rod- and cube-shaped AuNPs were detected few extremely. In addition, the sphere-shaped AuNPs were found in all of the four organs, and highest in the liver, moderate in spleen, but lowest in lung and kidney. In the light of these results we therefore concluded that the distribution of AuNPs *in vivo* was also suggested to be associated with the shape of AuNPs.

The presence of AuNPs in organs was also confirmed by TEM. Figure 7 showed typical TEM images of the ultrastructural features of liver cells exposed to sphere- (Fig. 7(a)), cube- (Fig. 7(b)), and rod-shaped AuNPs (Fig. 7(c)), respectively. The status of cells was completely normal as usual. It is found that nanoparticles were aggregated in the endosome, it appeared that the aggregation

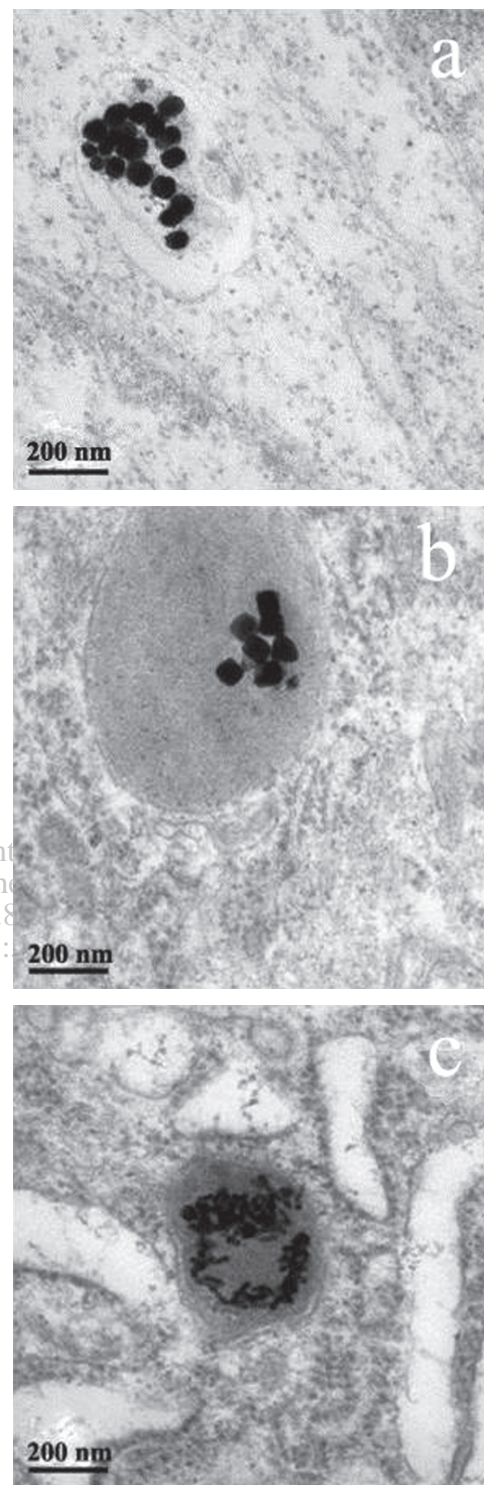


**Fig. 7.** TEM images of (a) sphere-, (b) cube-, and (c) rod-shaped AuNPs in liver cell after *i.v.* injection for 7 days.

one of the reasons for the difference in cellular uptake. For example, in our studies the cube-shaped AuNPs had the largest superficial area. It means cube-shaped could have had larger contact area with the cell membrane receptors which are free in blood, these adsorption of receptors will reduce the number of available receptor sites for binding in effect, therefore, the uptake of cube-shaped AuNPs in cell was low by comparison, we also speculated the difference in the surface chemistries between the spherical and rod/cube-shaped gold nanoparticles could be another effect factor. However, more studies will be required for further understanding of this detailed mechanism. These observations were consistent with the results in spleen (data not shown).

#### 4. CONCLUSIONS

In this work, we investigated the effect of AuNPs shape on their *in vivo* acute toxicological effects and biodistribution. The toxicity *in vivo* studies had demonstrated the optimal shape of AuNPs for biomedical applications was spherical, then the cube-shaped, followed the rod-shaped AuNPs. *In vivo* biodistribution tests revealed all AuNPs were preferentially accumulated in organ of liver and spleen which further proved that the shapes of AuNPs had an important effect on biodistribution. Besides, through the experiment of hemolysis assay, we obtained the optimal concentration of  $10^9$  grain/ml of AuNPs for *in vivo* applications. We also observed the accumulation of AuNPs in cell prone to be related to the shape. Our results suggested AuNPs did undergo shape-dependent interaction with their *in vivo* acute toxicological effects and biodistribution. The finding from this study will shed new light on the designing of optimal AuNPs for biomedical applications.

**Acknowledgments:** This work was financially supported by the National Natural Science Foundation of China (30970733), National Basic Research Program of China (973 Program) (2007CB935603, 2010CB732402), and Program for New Century Excellent Talents in Fujian Province University.

#### References and Notes

- Y. Z. Huang, W. Z. Wang, H. Y. Liang, and H. X. Xu, *Cryst. Growth. Des.* 9, 858 (2009).
- R. Sardar, A. M. Funston, P. Mulvaney, and R. W. Murray, *Langmuir* 25, 13840 (2009).
- D. J. Maxwell, J. R. Taylor, and S. M. Nie, *J. Am. Chem. Soc.* 124, 9606 (2002).
- A. K. Salem, P. C. Searson, and K. W. Leong, *Nat. Mater.* 2, 668 (2003).
- M. S. Han, A. K. R. Lytton-Jean, B. K. Oh, J. Heo, and C. A. Mirkin, *Angew. Chem. Int. Edit.* 45, 1807 (2006).
- Z. X. Wang and L. Ma, *Coordin. Chem. Rev.* 253, 1607 (2009).
- X. H. Huang, P. K. Jain, I. H. El-Sayed, and M. A. El-Sayed, *Nanomedicine* 2, 681 (2007).
- X. H. Huang, I. H. El-Sayed, W. Qian, and M. A. El-Sayed, *J. Am. Chem. Soc.* 128, 2115 (2006).
- C. M. Cobley and Y. N. Xia, *Elements* 5, 309 (2009).
- B. D. Chithrani, A. A. Ghazani, and W. C. W. Chan, *Nano Lett.* 6, 662 (2006).
- W. Jiang, B. Y. S. Kim, J. T. Rutka, and W. C. W. Chan, *Nat. Nanotechnol.* 3, 145 (2008).
- B. D. Chithrani and W. C. W. Chan, *Nano Lett.* 7, 1542 (2007).
- G. D. Zhang, Z. Yang, W. Lua, R. Zhang, Q. Huang, M. Tian, L. Li, D. Liang, and C. Li, *Biomaterials* 30, 1928 (2009).
- A. Verma, O. Uzun, Y. H. Hu, Y. Hu, H. Han, N. Watson, S. L. Chen, D. J. Irvine, and F. Stellacci, *Nat. Mater.* 7, 588 (2008).
- S. G. Wang, W. T. Lu, O. Tovmachenko, U. S. Raia, H. T. Yua, and P. C. Ray, *Chem. Phys. Lett.* 463, 145 (2008).
- W. Cho, M. Cho, J. Jeong, M. Choi, H. Y. Cho, B. S. Han, S. H. Kim, H. O. Kim, Y. T. Lim, B. H. Chung, and J. Jeong, *Toxicol. Appl. Pharmacol.* 236, 16 (2009).
- W. H. D. Jong, W. I. Hagens, P. Krystek, M. C. Burger, A. J. A. M. Sips, and R. E. Geertsma, *Biomaterials* 29, 1912 (2008).
- Y. Pan, S. Neuss, A. Leifert, M. Fischler, F. Wen, U. Simon, G. Schmid, W. Brandau, and W. Jahnens-Dechent, *Small* 3, 1941 (2007).
- M. Semmler-Behnke, W. G. Kreyling, J. Lipka, S. Fertsch, A. Wenk, S. Takenaka, G. Schmid, and W. Brandau, *Small* 4, 2108 (2008).
- G. Sonavane, K. Tomoda, and K. Makino, *Colloid. Surface. B* 66, 274 (2008).
- C. J. Murphy, A. M. Gole, J. W. Stone, P. N. Sisco, A. M. Alkilany, E. C. Goldsmith, and S. C. Baxter, *Acc. Chem. Res.* 41, 1721 (2008).
- H. C. Fischer and W. C. W. Chan, *Curr. Opin. Biotech.* 18, 565 (2007).
- A. Whitehead and N. Stallard, *ATLA-Altern. Lab. Anim.* 32, 73 (2004).
- United States Pharmacopeial Convention, United States Pharmacopeia, 24, United States Pharmacopeial Convention, Rockville (MD) (2000).
- N. Lewinski, V. Colvin, and R. Drezek, *Small* 4, 26 (2008).
- L. R. Hirsch, J. B. Jackson, A. Lee, N. J. Halas, and J. L. West, *Anal. Chem.* 75, 2377 (2003).
- P. A. Botham, *ATLA-Altern. Lab. Anim.* 30, 185 (2002).
- X. L. Huang, B. Zhang, L. Ren, S. F. Ye, L. P. Sun, Q. Q. Zhang, M. C. Tan, and G. M. Chow, *J. Mater. Sci-Mater. M* 19, 2581 (2008).
- H. Ohtsuki, K. Yoshifumi, H. Satoshi, K. Reika, and H. Yoshihiro, *Ophthalmologica* 214, 105 (2000).
- T. M. Saba, *Arch. Intern. Med.* 126, 1031 (1970).

Received: 5 March 2010. Revised/Accepted: 10 March 2010.